Selective Electroless Plating of 3D-Printed Plastic Structures for Three-Dimensional Microwave Metamaterials

Atsushi Ishikawa,[1,a)] Taiki Kato,[1] Nobuyuki Takeyasu,[2] Kazuhiro Fujimori,[1] and Kenji Tsuruta[1]

[1]*Department of Electrical and Electronic Engineering, Okayama University, 3-1-1 Tsushimanaka, Kitaku, Okayama 700-8530, Japan*

[2]*Department of Chemistry, Okayama University, 3-1-1 Tsushimanaka, Kitaku, Okayama 700-8530, Japan*

A technique of selective electroless plating onto PLA-ABS (Polylactic Acid-Acrylonitrile Butadiene Styrene) composite structures fabricated by three-dimensional (3D) printing is demonstrated to construct 3D microwave metamaterials. The reducing activity of the PLA surface is selectively enhanced by the chemical modification involving Sn^{2+} in a simple wet process, thereby forming a highly conductive Ag-plated membrane only onto the PLA surface. The fabricated metamaterial composed of Ag-plated PLA and non-plated ABS parts is characterized experimentally and numerically to demonstrate the important bi-anisotropic microwave responses arising from the 3D nature of metallodielectric structures. Our approach based on a simple wet chemical process allows for the creation of highly complex 3D metal-insulator structures, thus paving the way toward the sophisticated microwave applications of the 3D printing technology.

[a)] Electronic mail: a-ishikawa@okayama-u.ac.jp.

Additive manufacturing, commonly known as three-dimensional (3D) printing, has become rapidly spread over recent years, offering a new capability to produce 3D objects not only for industrial application but also for private use.[1] Among several printing methods, fused deposition modeling is the most common one, where complex 3D plastic structures can be readily obtained by laying down thermoplastic resin, e.g., PLA and ABS, in a layer-by-layer fashion.[2] By metalizing the surface of 3D-printed structures via an additional coating process, conductive components with relatively light weight were also realized, finding potential application in microwave devices, such as waveguides, filters, and antennas.[3-5] There, electroless plating is the most cost-effective and suitable technique for the metal deposition onto insulating plastics, since it can be chemically performed without applying an external electrical potential.[6] Different from other methods, such as vacuum evaporation and sputtering, the entire surface including shaded/occluded areas of 3D structures can be uniformly plated with various kinds of metal in a simple wet chemical process.[7-9] Although electroless plating achieves robust and scalable metallization for different systems,[10-12] selective plating onto the specific predefined areas of 3D-printed structures remains a major challenge.

Electromagnetic metamaterials have achieved massive breakthrough and application from microwave to optics, being one of the major fields over the past decades.[13-16] Based on flexible design of building blocks in metamaterials, one can fully engineer their resonant and dispersive properties, thereby demonstrating fascinating phenomena and functionalities, such as artificial magnetism, negative refractive index, and cloaking.[17-22] Especially in the microwave metamaterials, considerable progress has been made toward their practical applications in advanced communication and remote sensing technologies.[23-26] While microwave metamaterials have been naturally developed in a two-dimensional platform using a printed circuit board,[27,28] quasi 3D versions were also demonstrated by assembling circuit boards in 3D space to exploit bulk isotropic property.[29,30] More recently, by using fully-metalized 3D-printed structures, truly 3D metamaterials have been reported to demonstrate sophisticated functionalities, such as a self-supporting low loss lens and broadband optical activity.[31,32] On the other hand, to gain higher design flexibility of such metamaterials, integration of conductive metallic and insulating plastic parts into a device is highly desirable and ideally may be accomplished within the plating process.[33,34]

Here, we present a technique of selective electroless plating onto PLA-ABS composite structures fabricated by 3D printing. The greatest advantage of our technique is that 3D metal-insulator composite structures can be formed directly by a simple wet chemical process of 3D-printed structures. To prove the broad benefit of our technique, we fabricate a 3D microwave metamaterial consisting of self-standing split-ring resonators (SRRs) and demonstrate the important bi-anisotropic responses arising from the 3D nature of metallodielectric structures. Our approach allows for the creation of highly complex 3D metal-insulator structures, thus opening up the avenues for versatile applications of the 3D printing technology.

Figure 1 shows the process of our selective electroless plating, consisting of different 6 steps in series: (a) a PLA (white part) -ABS (yellow part) composite structure was firstly fabricated by using a 3D printer (3D systems, CubeX Duo), and then (b) immersed into a 0.1 mol/L acidic stannous chloride ($SnCl_2$) aqueous solution for 2 hours at room temperature.[35] Since the adhesion between Ag nanoparticles and the PLA/ABS surface is very weak due to their surface energy difference,[36] Ag plating cannot be achieved without appropriate surface chemical modification. In this process,

the whole surface of the PLA-ABS composite is uniformly covered with Sn^{2+}, which acts as a reducing active site to dramatically improve Ag nucleation and adhesion in the subsequent plating process.[37] (c) Based on the solubility difference between PLA and ABS in Acetone, the Sn^{2+} on the ABS surface was selectively washed away within 5 minutes by the Acetone post-cleaning process. (d) The electroless plating was then performed by immersing the sample into a 0.15 mol/L ammoniacal silver nitrate ($AgNO_3$) aqueous solution, and (e) this process was accelerated by adding a 1.0 mol/L glucose ($C_6H_{12}O_6$) aqueous solution as a reducing agent. During these processes, Ag^+ was reduced only on the PLA surface to produce Ag crystal nuclei and they grow quickly as Ag nanoparticles to form a thick plated membrane. After keeping the reaction temperature at 60 ºC for a half hour, (f) the sample was completed by washing with deionized water and dried with desiccated nitrogen.

Based on the aforementioned chemical process, we fabricated a 3D microwave metamaterial consisting of self-standing SRRs, which are typical building blocks to exhibit artificial magnetic responses.[38,39] Figs. 2(a) and 2(b) show photographs of a metamaterial consisting of 3 × 3 PLA-SRRs on an ABS substrate before and after the

selective electroless plating. The schematic unit cell of the metamaterial is also shown in Fig. 2(c) where the unit cell area, $p_x \times p_y$, the SRR diameter, d, width, w, thickness, t, and gap size, g, were 20×20 mm^2, 14 mm, 4 mm, 3 mm, and 2.5 mm respectively. Through the plating process, only the PLA-SRRs (white part) became metallic color, while the ABS substrate (yellow part) remained the same with slight change of the surface texture due to the dissolution in Acetone. Fig. 2(d) shows the cross-sectional scanning electron microscopy (SEM) image of the Ag-plated PLA surface, revealing that a 50-μm plated membrane is uniformly formed by the aggregation of Ag nanoparticles. These observations indicate that a highly conductive Ag-plated membrane was formed only on the PLA surface, not on the ABS one, demonstrating the creation of highly complex 3D metal-insulator structures by a simple wet chemical process. Since the membrane thickness is much larger than the skin depth, which is about 1 μm at microwave frequencies, the internal PLA structure is fully shielded from the incident microwave. On the other hand, the surface roughness of the membrane naturally increases the surface resistance to limit the microwave performance. However, our preliminary microwave measurement (see Supplementary Fig. S1) proved that the

Ag-plated PLA surface exhibited a fairly high reflectance up to 86.9% at the C-band (4 - 8 GHz), thus our technique may be applicable to the microwave device applications.

To characterize the microwave responses of the fabricated metamaterial, the transmission measurement was performed in free space by using a network analyzer (Agilent Technologies, 8722ES). Two identical linear-polarized patch antennas[40] operating at 5.5 GHz were fabricated using a Rogers 4350B laminate and placed facing each other with the sample in between. There, the sample was carefully positioned in the far-field region along the normal axis of the patch's plane where the sample was illuminated by a plane wave. The measurement setup was then calibrated such that T = 100% for a bare ABS substrate in the measured frequency range. Figure 3(a) shows the measured transmittance spectra of the metamaterial for the sample rotation of $\theta = 0^{o}$ and $\theta = 90^{o}$. Some data exceeded T = 100% of the reference ABS substrate, but they were still within a noise level. At $\theta = 0^{o}$, where the incident electric filed was parallel to the SRR gap, a typical resonant dip was clearly observed at ~ 5 GHz. When rotating the sample at $\theta = 90^{o}$, on the other hand, the resonant dip totally disappeared, exhibiting a strong anisotropic property of the 3D SRRs. Fig. 3(b) shows the numerically simulated

transmittance spectra based on a finite element method (FEM), which well re-produced the experimental results qualitatively and quantitatively. In the calculations, we used $\varepsilon_{ABS} = 3.0$ and the empirical value for ε_{Ag},[41] with a damping constant 5 times larger than the bulk value to take into account the additional electron scattering in Ag nanoparticles of the plated membrane. The discrepancy between the experimental and numerical results can be attributed to a minor deformation of the 3D-printed structures caused by the chemical process. Note that the additional simulation result of the non-plated 3D SRRs (see Supplementary Fig. S2) showed no such a strong anisotropic property, and this also proved that the PLA surface was surely metallized to exhibit a pronounced electromagnetic resonance.

It is known that the SRR has both electric and magnetic dipole moments; the electric dipole moment is given by the separated charges within the gap, while the magnetic one is given by the current circularly flowing along the ring. In the case of the 3D SRR with a single gap, the inversion symmetry is broken along the propagation direction (the z-axis); therefore, it exhibits strong bi-anisotropic property, where electric and magnetic resonances are excited simultaneously by the incident electric and

magnetic fields. Figures 4(a) and 4(b) show the numerically simulated E_x and H_y distributions in the x-z plane of the 3D SRR at the resonance, f = 4.98 GHz. The incident electric field excites an electric dipole moment within the gap, which induces a circular current in the ring [Fig. 4(a)]. At the same time, a magnetic dipole moment perpendicular to the ring is also excited not only by the circular current but also by the incident magnetic field [Fig. 4(b)]. Such a bi-anisotropic response of the relevant electric and magnetic fields in the system can be described by the following expression.[42]

$$\begin{pmatrix} D \\ B \end{pmatrix} = \begin{pmatrix} \varepsilon_0\varepsilon & -i\xi/c_0 \\ i\xi/c_0 & \mu_0\mu \end{pmatrix} \begin{pmatrix} E \\ H \end{pmatrix} \quad (1)$$

where ε_0 (μ_0) is the vacuum permittivity (permeability), ε (μ) is the effective permittivity (permeability), c_0 is the speed of light, and ξ in the off-diagonal terms is the bi-anisotropy parameter to describe the excitation of electric dipole by the magnetic field and vice versa. By taking into account this bi-anisotropic response, the effective parameters, ε, μ, and ξ, of the metamaterial were retrieved from the numerical results as shown in Figs. 4(c) and 4(d). At the resonance, a strong Lorentzian-like dispersion was

clearly observed in ε, reaching a negative value within a certain frequency range. The magnetic response, μ, on the other hand, was relatively weak, but still exhibited similar dispersion with the values away from 1.0 near the resonance. Strong electric and weak magnetic resonances can be naturally understood by considering a large capacitance and a small inductance of the SRR structure. In the same frequency region, typical anti-resonant dispersion was also observed for the bi-anisotropy, ξ, which interrelated the electric and magnetic responses. Depending on the values of Re[ξ] and Im[ξ], the electric (magnetic) dipole is excited by the magnetic (electric) field with different strengths and phases. Note that such a bi-anisotropic response arises from the 3D nature of the fabricated metamaterial, where the inversion symmetry of the system is broken. The overall response of the metamaterial, i.e., the complex refractive index n, can be obtained from the relationship $n^2 = \varepsilon\mu - \xi^2$, and is shown in Fig. 4(d). Here, the root was chosen such that Im(n) $\geq$ 0 to satisfy the energy conservation in a passive material. In addition to the pure electric and magnetic responses of the 3D SRR, their mutual coupling, ξ, played a dominant role in their resonant behavior, hence, the real part of the refractive index showed a large swing from 0.27 to 2.0 at microwave frequencies.

In conclusion, a technique of selective electroless plating onto PLA-ABS composite structures fabricated by 3D printing was proposed and demonstrated. We applied our technique to fabricate a 3D microwave metamaterial consisting of self-standing SRRs and characterized their microwave responses. The corresponding numerical simulation qualitatively and quantitatively re-produced the experimental results, revealing the important bi-anisotropic responses arising from the 3D nature of the fabricated metamaterial. The 3D SRR demonstrated here is a simple example, but our technique can be extended to mass production of highly complex 3D metal-insulator structures. Hence, it may hold great promise for the versatile microwave and mechanical applications of the 3D printing technology.

See supplementary material for the reflection measurement of Ag-plated PLA plates and the simulation result of the non-plated 3D SRRs.

This work was supported in part by the JSPS KAKENHI Grant Number 15KK0237. The authors gratefully thank the Division of Instrumental Analysis,

Okayama University for the SEM measurement and Mr. K. Hashimoto for his assistance in the experiment.

REFERENCES

[1] Hideo Kodama, Rev. Sci. Instrum. **52**, 1770 (1981).

[2] I. Gibson, D. Rosen, and B. Stucker, *Additive Manufacturing Technologies: 3D Printing, Rapid Prototyping, and Direct Digital Manufacturing* (Springer-Verlag, New York, 2015).

[3] M. Vaezi, H. Seitz, and S. Yang, Int. J. Adv. Manufact. Technol. **67**, 1721 (2013).

[4] M. D'Auria, W. J. Otter, J. Hazell, B. T. W. Gillatt, C. Long-Collins, N. M. Ridler, and S. Lucyszyn, IEEE Trans. Comp. Pack. Manuf. Technol. **5**, 1339 (2015).

[5] C. Guo, X. Shang, M. J. Lancaster, and J. Xu, IEEE Microw. Compon. Lett. **25**, 442 (2015).

[6] G. O. Mallory and J. B. Hajdu, *Electroless Plating: Fundamentals and Applications* (American Electroplaters and Surface Finishers Society, Orland, FL, 1990).

[7] P.-C. Yen, Polymer **36**, 3399 (1995).

[8] A. A. Antipov, G. B. Sukhorukov, Y. A. Fedutik, J. Hartmann, M. Giersig, and H. Mohwald, Langmuir **18,** 6687 (2002).

[9] N. Takeyasu, T. Tanaka, and S. Kawata, Jpn. J. Appl. Phys. **44**, L1134 (2005).

[10] F. Formanek, N. Takeyasu, T. Tanaka, K. Chiyoda, A. Ishikawa, and S. Kawata, Appl. Phys. Lett. **88**, 083110 (2006).

[11] A. Radke, T. Gissibl, T. Klotzbucher, P. V. Braun, and H. Giessen, Adv. Mater. **23**, 3018 (2011).

[12] T. A. Schaedler, A. J. Jacobsen, A. Torrents, A. E. Sorensen, J. Lian, J. R. Greer, L. Valdevit, and W. B. Carterl, Science **334**, 962 (2011).

[13] D. R. Smith, J. B. Pendry, and M. C. K. Wiltshire, Science **305**, 788 (2004).

[14] C. M. Soukoulis, S. Linden, and M. Wegener, Science **315**, 47 (2007).

[15] N. I. Zheludev, Science **328**, 582 (2010).

[16] N. I. Zheludev and Y. S. Kivshar, Nat. Mater. **11**, 917 (2012).

[17] A. Ishikawa, T. Tanaka, and S. Kawata, Appl. Phys. Lett. **91**, 113118 (2007).

[18] W. Cai, U. K. Chettiar, A. V. Kildishev, and V. M. Shalaev, Nat. Photon. **1**, 224 (2007).

[19] J. Valentine, S. Zhang, T. Zentgraf, E. Ulin-Avila, D. A. Genov, G. Bartal, and X. Zhang, Nature, **455**, 376 (2008).

[20] N. Liu, L. Langguth, T. Weiss, J. Kastel, M. Fleischhauer, T. Pfau, and H. Giessen, Nat. Mater. **8**, 758, (2009).

[21] J. K. Gansel, M. Thiel, M. S. Rill, M. Decker, K. Bade, V. Saile, G. von Freymann, S. Linden, M. Wegener, Science **325**, 1513 (2009).

[22] A. Ishikawa and T. Tanaka, Sci. Rep. **5**, 12570 (2015).

[23] I. Bulu, H. Caglayan, K. Aydin, and E. Ozbay, New J. Phys. **7**, 223 (2005).

[24] E. Lier, D. H. Werner, C. P. Scarborough, Q. Wu, and J. A. Bossard, Nat. Mater. **10**, 216 (2011).

[25] J. Hunt, T. Driscoll, A. Mrozack, G. Lipworth, M. Reynolds, D. Brady, D. R. Smith, Science **339**, 310 (2013).

[26] J. Hunt, J. Gollub, T. Driscoll, G. Lipworth, A. Mrozack, M. S. Reynolds, D. J. Brady, and D. R. Smith, J. Opt. Soc. Am. A **31**, 2109 (2014).

[27] D. R. Smith, Willie J. Padilla, D. C. Vier, S. C. Nemat-Nasser, and S. Schultz, Phys. Rev. Lett. **84**, 4184 (2000).

[28] A. Grbic and G. V. Eleftheriades, Phys. Rev. Lett. **92**, 117403 (2004).

[29] R. A. Shelby, D. R. Smith, and S. Schultz, Science **292**, 77 (2001).

[30] D. Schurig, J. J. Mock, B. J. Justice, S. A. Cummer, J. B. Pendry, A. F. Starr, and D. R. Smith, Science **314**, 977 (2006).

[31] I. M. Ehrenberg, S. E. Sarma, and B.-I. Wu, Appl. Phys. Lett. **112**, 073114 (2012).

[32] H. S. Park, T.-T. Kim, H.-D. Kim, K. Kim, and B. Min, Nat. Commun. **5**, 5435 (2014).

[33] R. A. Farrer, C. N. LaFratta, L. Li, J. Praino, M. J. Naughton, B. E. A. Saleh, M. C. Teich, and J. T. Fourkas, J. Am. Chem. Soc. **128**, 1796 (2006).

[34] N. Takeyasu, T. Tanaka, and S. Kawata, Appl. Phys. A **90**, 205 (2008).

[35] Y. Kobayashi, V. Salgueiriño-Maceira, and L. M. Liz-Marzán, Chem. Mater. **13**, 1630 (2001).

[36] L. J. Gerenser, J. Vac. Sci. Technol. A **8**, 3682 (1990).

[37] J. E. Gray, P. R. Norton, and K. Griffiths, Thin Solid Films **484**, 196 (2005).

[38] J. B. Pendry, A. J. Holden, D. J. Robbins, and W. J. Stewart, IEEE Trans. Microwave Theory Tech. **47**, 2075 (1999).

[39] C.-C. Chen, A. Ishikawa, Y.-H. Tang, M.-H. Shiao, D. P. Tsai, and T. Tanaka, Adv. Opt. Mater. **3**, 44 (2015).

[40] I. J. Bahl, Microwave **18**, 50 (1979).

[41] P. B. Johnson and R. W. Christy, Phys. Rev. B **6**, 4370 (1972).

[42] C. E. Kriegler, M. S. Rill, S. Linden, and M. Wegener, IEEE J. Sel. Top. Quantum Electron. **16**, 367 (2010).

FIGURES

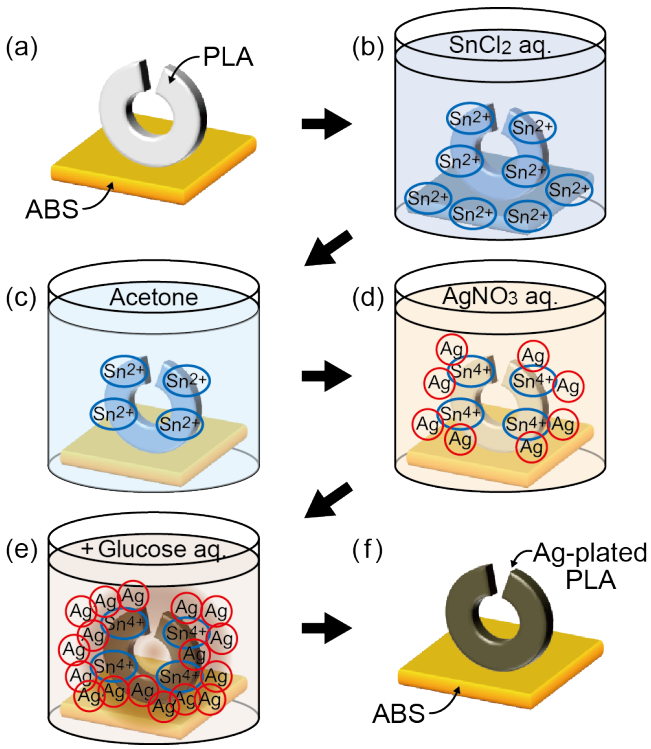

FIG 1. Process of selective electroless plating: (a) PLA (white part) –ABS (yellow part) composite structure fabricated by 3D printing, (b) $SnCl_2$ surface pre-treatment to form the reducing active Sn^{2+} sites for Ag deposition, (c) Acetone post-cleaning to remove Sn^{2+} only from the ABS surface, (d) Selective Ag deposition onto the PLA surface by the electroless plating, (e) Glucose reductant solution added to accelerate the plating process, and then (f) Washed with deionized water and dried.

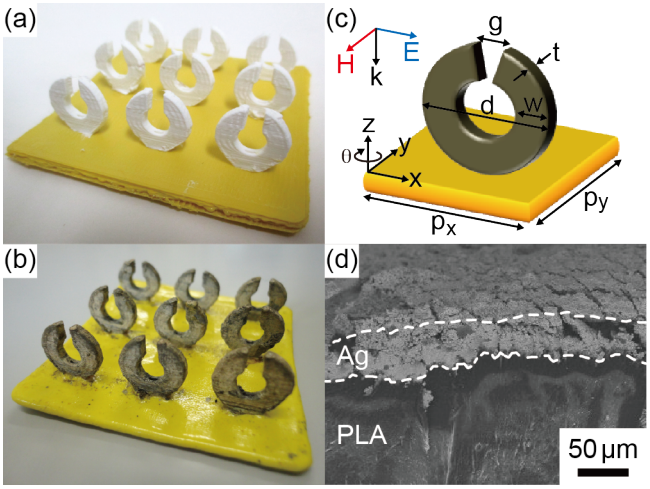

FIG 2. Photographs of the fabricated metamaterial consisting of 3 × 3 PLA-SRRs on an ABS substrate (a) before and (b) after the selective electroless plating. (c) Schematic unit cell of the metamaterial for the sample rotation of $\theta = 0^{o}$ where the incident electric field is parallel to the SRR gap. The unit cell area, $p_x \times p_y$, the SRR diameter, d, width, w, thickness, t, and gap size, g, were 20 × 20 mm^2, 14 mm, 4 mm, 3 mm, and 2.5 mm respectively. (d) Cross-sectional SEM image of the Ag-plated PLA surface, revealing that a 50-μm plated membrane is uniformly formed by the aggregation of Ag nanoparticles.

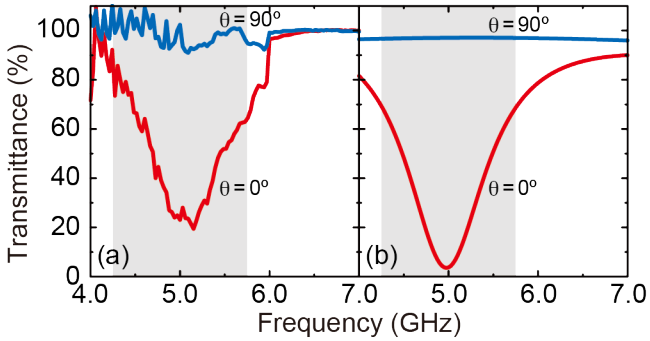

FIG 3. (a) Measured transmittance spectra of the metamaterial at θ = 0º and θ = 90º. (b) Numerically simulated transmittance spectra, which well re-produced the experimental results qualitatively and quantitatively.

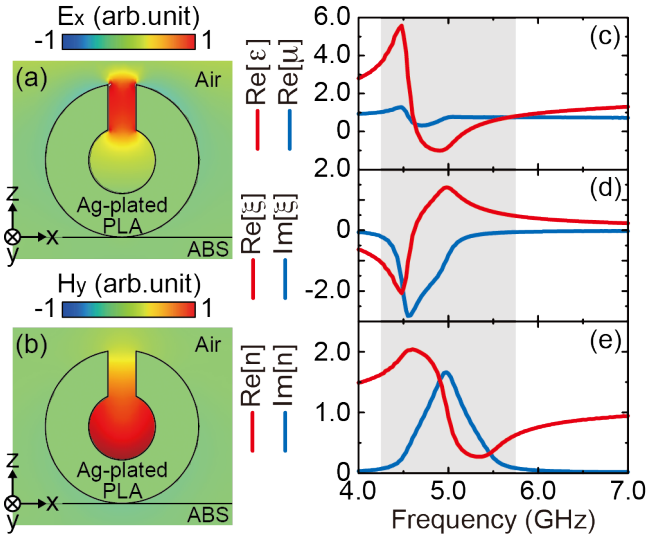

FIG 4. Numerically simulated (a) E_x and (b) H_y distributions in the x-z plane at the resonance, f = 4.98 GHz. Real and imaginary parts of the retrieved effective parameters of the metamaterial: (c) permittivity, ε, and permeability, μ, (d) bi-anisotropy parameter, ξ, and (e) refractive index, n.